Electrochimica Acta 283 (2018) 997–1005

Contents lists available at ScienceDirect

Electrochimica Acta

journal homepage: www.elsevier.com/locate/electacta

Carbonous metallic framework of multi-walled carbon Nanotubes/ Bi_2S_3 nanorods as heterostructure composite films for efficient quasi-solid state DSSCs

Anam Ali Memon [a, f], Supriya A. Patil [b, c], Kyung Chul Sun [d, e], Naveed Mengal [a, f], Alvira Ayoub Arbab [a, f], Iftikhar Ali Sahito [f], Sung Hoon Jeong [a, *], Hak Sung kim [b, c, **]

[a] *Department of Organic and Nano Engineering, Hanyang University, Seoul, 133-791, South Korea*
[b] *Department of Mechanical Engineering, Hanyang University, Haengdang-dong, Seongdong-gu, Seoul, 133-791, South Korea*
[c] *Institute of Nano Science and Technology, Hanyang University, Seoul, 133-791, South Korea*
[d] *Department of Fuel Cells and Hydrogen Technology, Hanyang University, Seoul, 133-791, South Korea*
[e] *Research Institute of Industrial Technology Convergence Technical Textile and Materials R&D Group, Korea Institute of Industrial Technology, South Korea*
[f] *Department of Textile Engineering, Mehran University of Engineering and Technology, Pakistan*

ARTICLE INFO

Article history:
Received 8 December 2017
Received in revised form
10 March 2018
Accepted 18 April 2018
Available online 21 April 2018

Keywords:
Bi_2S_3 nanorods (NRs)
Multi-walled carbon nanotubes (MWCNTs)
Carbonous metallic heterostructure composite film (CMHCs)
Quasi-solid state dye-sensitized solar cells (QDSSCs)

ABSTRACT

Bismuth sulfide (Bi_2S_3); is a non-toxic metal chalcogenide and a promising semiconductor in energy storage devices, but it has not received much attention in the regime of dye sensitized solar cells (DSSCs). The present research describes the synthesis of highly electro-catalytic active counter electrode (CE) material for quasi-solid state dye sensitized solar cells (QDSSCs), namely carbonous metallic heterostructure composite (CMHC), composed of solution processed bismuth sulfide nanorods and modified Multi walled carbon nanotubes (MWCNTs). Due to the positive synergistic effect of conductive MWCNT network and rod-like morphology of bismuth sulfide, the composite exhibits multifunctional characteristics of high conductivity, superior electro-catalytic activity and optimal porosity. The carbonous composite with a dominant oxygen rich surface shows enhanced electro-catalytic activity, low charge transfer resistance (R_{CT}), and exceptional cyclic stability as compared with pristine bismuth sulfide. The as-synthesized composite exhibit a very low charge transfer resistance of 0.9 Ω which signifies a fast electron transport mechanism. The suggested composite CE with 3% polymer gel electrolyte achieves a high efficiency of 8.24% comparable to Pt (8.47%). Based on the facile synthesis of composites and excellent performance of CE, the designed quasi-solid state dye sensitized solar cells stand out as an efficient next generation solar cells.

1. Introduction

The evolution of renewable energy technologies based on low-cost and sustainable elements is a prerequisite to develop solutions for increasing energy demands. Dye-sensitized solar cells (DSSCs) are among the existing renewable energy technologies and have been extensively investigated due to their eco-friendly, low-cost, facile fabrication, and comparatively high PCE properties compared to conventional solar cells [1,2]. Moreover, from both technical and economic standpoints, DSSCs have great potential for large scale applications [3]. The DSSC assembly pioneered by Gratzel employs a dye-sensitized TiO_2 film as the photo anode, a liquid/solid electrolyte containing a redox system, and a catalyst-coated conductive substrate as the counter electrode (CE) [4]. Among all, the counter electrode plays an important role in the regeneration of iodide and electron transfer at the interface between the electrolyte and electrode. Therefore, the design and fabrication of suitable CE materials require both high conductivity and superior catalytic activity [5] [6]. Conventionally, platinized FTO has been used as a functional CE in DSSCs due to the excellent electro-catalytic activity and high conductivity of Pt [7].

---

[*] Corresponding author. Department of Organic and Nano Engineering, Hanyang University, Seoul, 133-791, South Korea.

[**] Corresponding author. Department of Mechanical Engineering, Hanyang University, Haengdang-dong, Seongdong-gu, Seoul, 133-791, South Korea.

E-mail addresses: shjeong@hanyang.ac.kr (S.H. Jeong), kima@hanyang.ac.kr (H.S. kim).

https://doi.org/10.1016/j.electacta.2018.04.131

Nevertheless, the selection of Pt as a CE material in DSSCs is argumentative due to its instability in iodine complex-based electrolytes, high cost [8] and scarcity. Additionally, Pt tends to induce the formation of polyiodides, which strongly reduce the photo conversion efficiency of DSSCs [9,10]. In this regard, diverse non-Pt CE materials have been designed and utilized in DSSCs such as polymorphs of carbon (carbon nanotubes [11,12], graphene [13] [3], and activated carbon [14]), inorganic compounds including transition metal chalcogenides [15] [16], oxides [17], carbides [18] nitrides [19], and conducting polymers [20].

However, it is difficult to achieve both a high electro-catalytic activity and elevated electrical conductivity in a single material. For example, transition metal chalcogenides possess good thermal stability and efficient electro-catalytic activity, but due to excessive grain boundaries and defects, their conductivity is comparatively low [21]. In addition, carbon materials are highly conductive in nature but exhibit a poor electro-catalytic activity. Similarly, conducting polymers are sufficiently unstable. Thus, the idea of fabricating heterostructure composites emerged, as it would take benefit of the components and their interaction, thus outperforming any single component [22].

Henceforth, by merging various carbon materials with other nanostructures, unique heterostructures with incredible and potentially unexpected opto-electronic properties can be generated. The carbon based heterostructures with metal sulfides are gaining much interest amongst researchers [23], as the subsequent heterostructures offer synchronized characteristics of excellent conductivity, superior electro-catalytic activity, and defect-rich morphology. Among different carbon materials, widely used multi-walled carbon nanotubes (MWCNTs) have emerged as a promising electronic composite material. MWCNTs provide fast electron transport due to the coexistence of a tubular morphology and diffusive transport [24]. They also exhibit good mechanical properties, which are also helpful for film formation [25]. Based on their remarkable properties and immense suitability in electronic composite materials, MWCNTs were assembled with a well-known transition metal sulfide, bismuth sulfide, in this study.

Bismuth sulfide (Bi_2S_3) is a renowned layered semiconductor with a direct band gap of 1.3 eV and it possesses the additional merits of a high absorption coefficient, superior photocatalytic activity, and reasonable conversion efficiency. In addition, Bi_2S_3 can be synthesized by easy, low energy consuming, and cost effective methods, which is favorable for its scalable application. However, very few groups have reported Bi_2S_3 as a CE material for dye-sensitized solar cells, despite its potential applications in super capacitors [26], lithium ion batteries [27,28], and hydrogen storage materials [29].

To the best of our knowledge, a heterostructure composite consisting of Bi_2S_3 with MWCNTs as a CE catalyst for DSSCs has yet to be reported. Pristine carbon materials usually exhibit good electrical conductivity but offer limited catalytic active sites due to their chemical inertness [11]. In contrast to pristine CNTs, the existence of metal nanoparticles within CNTs can promote electron transfer from the metal to the carbon walls, which can change the electronic structure and reduce the surface work function of the carbon walls, consequently enhancing the catalytic activity of the carbon walls.

Heterostructured materials with two different energy level systems play an important role in achieving electron hole separation. Furthermore, the coupling of MWCNT with Bi_2S_3 can reduce the electron-hole recombination and enhance the light absorption phenomenon.

Initially, researchers focused on and compared the catalytic activities of different facets within Bi_2S_3 by employing various techniques in view of its influence on photo electrochemical performances. The results demonstrated that Bi_2S_3 (130) had a better electrical conductivity and higher open circuit voltage compared to other facets, resulting in a PCE of 3.5% [30]. Nevertheless, the PCE achieved was comparatively lower and hence, Bi_2S_3 composites with carbon materials have been investigated. Li et al. fabricated Bi_2S_3 microspheres grown on graphene sheets via a two-step solvothermal method and employed them as an electro catalyst for the CE in DSSCs. The as-synthesized hybrid boosted the conversion efficiency to 5.5% [31]. The enhancement of the PCE is mainly attributed to the efficient electron transport network provided by graphene. Zuo et al. also designed low-cost porous bismuth sulfide carbon (Bi_2S_3-C) composite microspheres through a solvothermal route. The Bi_2S_3-C composite offered a low charge transfer resistance at the electrode/electrolyte interface and high catalytic ability with a power conversion efficiency of 6.72% [32].

In this study, we report the synthesis of an electro-catalytically active and high conductivity material based on Bi_2S_3 NRs and MWCNTs as a carbonous metallic heterostructure composite (CMHC). The Bi_2S_3 NRs were fabricated via a facile solution process, as reported in our previous work [15]. As the hydrophobic nature of MWCNTs has always hindered the robust interfacial interaction with other components, effective functionalization of the graphitic surface was carried out by mild acid treatment. This surface modification enhances the surface energy and conductivity and facilitates the binding sites. Also, the oxygen functional groups inevitably accompany defect formation without compromising the conjugation length of the MWCNTs. We fabricated different composites by varying the concentration of Bi_2S_3 NRs in the composite material. Based on the beneficial synergistic effects of solution-processed Bi_2S_3 and acid-treated MWCNTs, the QDSSC assembled with this composite material CE exhibited excellent electro-catalytic activity towards iodide triiodide reduction. The photovoltaic performance of the QDSSC fabricated with our suggested CE system demonstrated a PCE of 8.24%, which is comparable to the PCE of Pt (8.47%). Our designed CE electro-catalyst has the ability to entrap a larger quantity of gel electrolyte and offers rapid reduction of iodide ions, thus demonstrating a high efficiency. This effective strategy and facile fabrication route of the CMHC electrode paves the way to low-cost quasi-solid state dye-sensitized solar cells (QDSSC).

2. Materials

MWCNT powder (carbon content >90%, diameter of 110–170 nm, length of 5–9 μm, Sigma Aldrich Co.) was selected for the formation of the conductive matrix. Nitric acid (60%, Matsunoen Chemicals) was used for functionalization of the CNTs. Bismuth trichloride ($BiCl_3$) and thioacetamide (TAA) were purchased from Sigma Aldrich and used for the synthesis of the bismuth sulfide (Bi_2S_3NRs). For the formation of carbon paste, polymer carboxymethyl cellulose (sodium salt with a M_W of 250,000 g) was used as a binding agent. A conductive transparent glass (FTO TEC 8, Pilkington Co) substrate was utilized. Dye sensitizer N719, *cis*-diisothiocyanato-bis (2, 2'-bipyridyl 4, 4'dicarboxylato) ruthenium (II) bis (tetra butyl ammonium), was purchased from Ever Light Co. TiO_2 (P25 by Degussa Co.) with a size of 20 nm, which was used for the photo anodes. Ionomer surlyn with a thickness of 60 μm was purchased from Solaronix. Other laboratory grade reagents were purchased from Sigma Aldrich Co.

3. Synthesis of bismuth sulfide nano rods (Bi_2S_3 NRs)

Bismuth sulfide Bi_2S_3 NRs were synthesized via a reaction between bismuth chloride ($BiCl_3$) and thioacetamide (TAA) using a solution process method. In brief, in a typical synthesis, 50 ml of an ethanol solution with 0.1 M $BiCl_3$ was mixed with 0.3 M TAA, sealed in 50 ml Falcon tubes and heated at 70 °C for 12 h. The black precipitation in the bottom of Falcon tube were thoroughly washed with ethanol and dried at room temperature before further characterization [33].

4. Synthesis of the carbonous metallic heterostructure composite (CMHC) electro-catalyst

The CMHC for efficient counter electrodes was prepared by combining the Bi_2S_3 NRs with functionalized MWCNTs. For the functionalization, 1 g of MWCNT powder was added to 100 ml of nitric acid. The solution was sonicated at room temperature for 2 h so that the oxidative moieties can be introduced on the basal planes of the MWCNTs. Next, different weight percentages (0.4,0.8 and 1.2 wt %) of the Bi_2S_3 NR precipitate were simultaneously added to the mixture. The resultant mixture was stirred for 8 h to produce a uniform solution. The solution was diluted with 500 ml of DI water and vacuum filtered. It was then washed several times to neutralize the pH. Carboxymethyl cellulose was used to convert the filtered and dried cake of CMHC into a consistent paste. For this, CMHC thin films were fabricated by tape casting the CMHC paste on a FTO glass substrate. The preparation method of the CMHC-based CE is clearly illustrated in Fig. S1 and the weight ratios of Bi_2S_3 and M-CNT are shown in Table S1.

5. Preparation of the gel electrolyte

The gel electrolyte was prepared with the following composition: 0.6 M 1-butyl-3-methyl-imidazolium iodide (BMPII), 0.1 M Lithium iodide (LiI), 0.05 M Iodine (I_2), 0.1 M Guanidine thiocyanate (GuNCS), and 0.5 M 4-*tert*-Butylpyridine (TBP) in 5 ml of acetonitrile. For the gel electrolyte, 3% polyethylene oxide (M_w of 300,000) by weight was added to the liquid electrolyte. The resultant mixture was sonicated and stirred for 20 min.

6. DSSC fabrication

For the fabrication of the photo anodes, double-holed FTO glasses ($1.5 \times 1.5\ cm^2$) were cleaned with acetone, distilled water, and ethanol for 20 min each. P25 (anatase TiO_2) and G2 (rutile TiO_2) pastes were prepared by previously reported methods [34]. They were deposited on the FTO glass using double masking tape with a thickness of 18 μm. The titania paste was dried and sintered by gradually increasing the temperature. The photo anodes were dried at 70 °C for 30 min followed by high temperature sintering in a furnace with a consecutive temperature sequence of 325, 375, 450, and 500 °C for 5, 5, 15, and 15 min, respectively. $TiCl_4$ treatment of the glass was carried out before and after deposition of the paste. The annealed photo anodes were immersed in a 0.3 mM N719 dye solution for 12 h. The DSSCs were fabricated by sandwiching the dye-immersed photo anodes and CMHC-coated counter electrodes with 60 μm thick surlyn as a sealant and cell spacer. A 3% gel electrolyte was filled into the cell through a hole drilled into the photo anodes and sealed by surlyn and a cover glass. The proposed quasi-solid state DSSC assembly is schematically illustrated in Fig. 1.

7. Characterization and measurements

The surface morphologies and thicknesses of the composite films were characterized by field emission–scanning electron microscopy (FE-SEM, JEOL JSM-6700 F) with a very thin coating of Pt at an accelerating voltage of 15 kV. The dispersion of the CMHC was examined by transmission electron microscopy (TEM, JOEL JEM-2100 F) at an accelerating voltage of 200 kV. Fourier Transform infrared (FTIR) spectra were recorded in the ATR mode by using a Nicolet™ iS™ 10 FTIR spectrometer from Thermo Fisher Scientific Inc., USA. X-ray photoelectron spectroscopy (XPS) analysis was performed using a Multi Lab ESCA 2000 system VG from Thermo Scientific, USA utilizing mono chromatic Al Kα X-rays. The survey scans analyzed from 1200 to 0 eV revealed the overall elemental compositions of the samples. The crystal structures of the composites were evaluated by the X-ray diffraction patterns recorded on a Rigaku Denki X-ray generator (Rigaku, D/MAX-2500) using CuKα ($\lambda = 1.5418$ A°) in the 2Θ range of 10–80°. The acceleration voltage and tube current of the X-ray generator were 40 kV and 60 mA, respectively. Raman measurements were carried out using a Raman microscopy system (NRS-3100, JASCO, Japan). The Raman spectra were recorded in the range of 1000–4000 nm. The electrical resistance of the composite-coated substrates was measured by using a standard four point-probe head system method and an RM3000 resistivity test unit by Jandel Engineering, Switzerland.

The electro-catalytic activity of the CMHC-based counter electrode tri-iodide/iodide redox reaction was evaluated by cyclic voltammetry (CV). This analysis was performed using an electrochemical workstation (Bio Logic Co.) with a three electrode system at a scan rate of $20\ mV\ s^{-1}$. The CMHC-coated counter electrode was used as the working electrode, Pt wire was the counter electrode, and Ag/AgCl was employed as the reference electrode. The electrolyte was an acetonitrile solution containing 10 mM (Lithium iodide) LiI, 0.01 M (Lithium perchlorate) $LiClO_4$, and 1 mM (Iodine) I_2. The electrochemical impedance spectra (EIS) were recorded over the frequency range of 0.05 Hz–500 kHz using a symmetrical cell. The symmetrical cell was fabricated by assembling two identical counter electrodes with two 60 μm surlyn layers in between. Photocurrent-photo voltage (J-V) curves were measured by using a K101-Lab20 source measuring unit (Mac Science Co.) with a 160 W xenon arc lamp as the light source (spectral match of 0.75–1.25, non-uniformity of irradiance of ≤±2%, temporal instability of ≤±2%).

8. Results and discussion

The morphologies and compositions of the M-CNT, Bi_2S_3 NRs, and as-synthesized CMHCs observed by scanning electron microscopy (SEM) are illustrated in Fig. 2. The SEM images show the tubular shape of the M-CNTs and, rod-like structure of Bi_2S_3 NRs at various magnifications, respectively. The acid-modified MWCNTs exhibited an aggregated tubular carbon matrix, forming an efficient conductive network structure (Fig. 2a). Such an interwoven tubular morphology provides conductive pathways and thereby results in a high conductivity. On the other hand, the images in Fig. 2b-c reveal that the Bi_2S_3 NRs prepared via the facile solution process method grew independently, and in irregular pattern. Low magnification scanning electron microscopy (SEM) images show that the Bi_2S_3 samples are composed of well segregated NRs with diameters of 10–90 nm. The length of the Bi_2S_3 NRs varied from several nanometers to around 1 mm. The high magnification SEM image reveals that the surface of each nanorod (NR) appears to be smooth with a rectangular tip, representing a well crystallized and rod-like morphology. Fig. 2d shows that our proposed electro-catalyst CMHC, prepared by the combination of solution-processed Bi_2S_3 and M-CNTs, possesses a smooth and crack-free coating on FTO glass. In the CMHC, the M-CNTs are well decorated with the Bi_2S_3 NRs (Fig. 2e-f). Interestingly, the CMHC structure offers few voids, which are suitable for the penetration of a large volume of gel electrolyte for the tri-iodide reduction reaction. The CMHC exhibits multifunctional characteristics including a high conductivity, superior electro-catalytic activity, and optimal porosity.

The dilute solution of CMHC was dropped over a TEM grid and

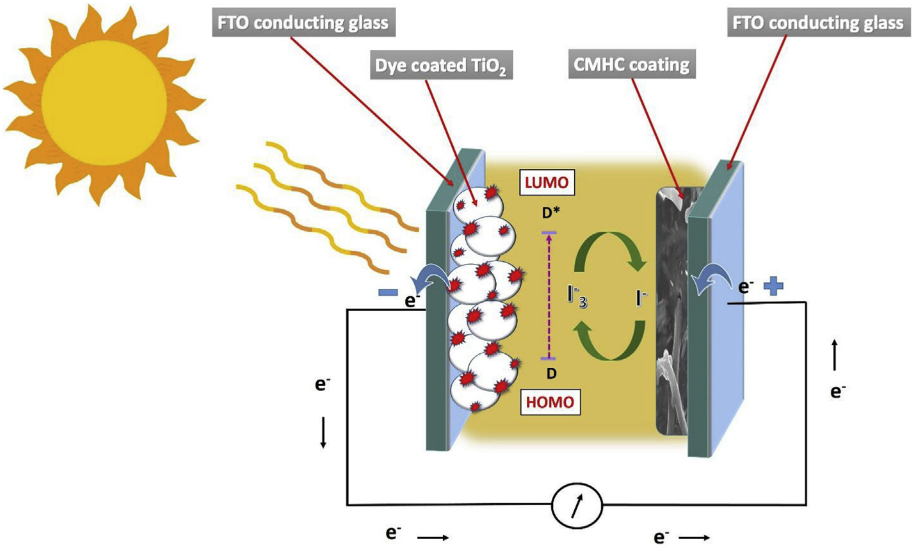

Fig. 1. Schematic illustration of CMHC CE based DSSC assembly.

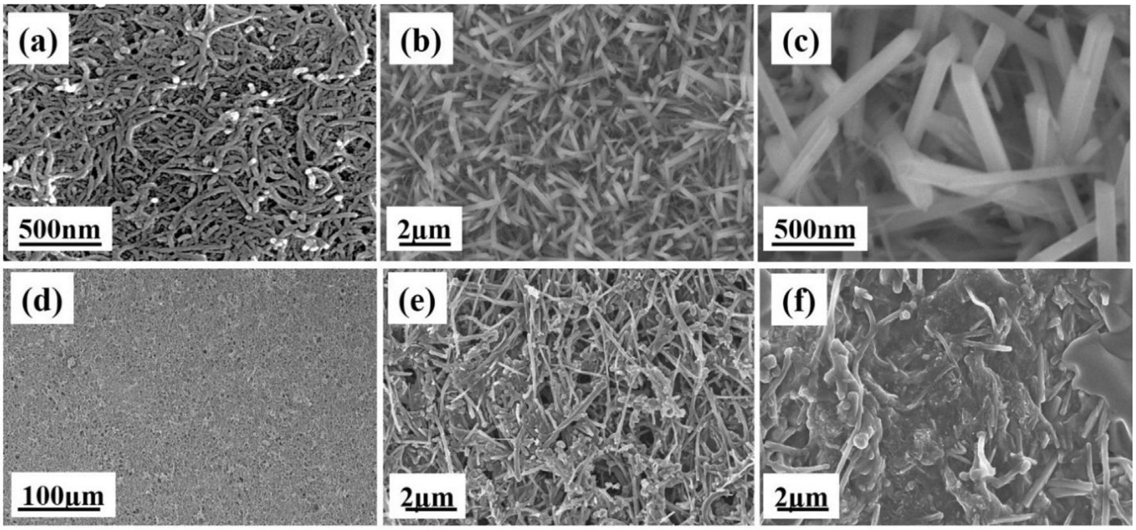

Fig. 2. SEM images of (a) acid-treated MWCNTs, (b–c) as-synthesized Bi_2S_3 NRs, and (d–f) CMHC films obtained at low and high magnifications.

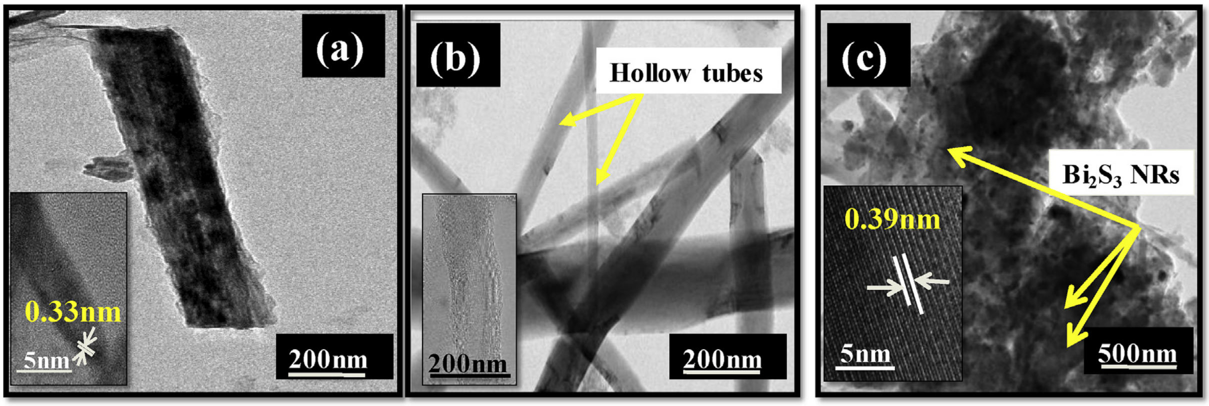

Fig. 3. TEM images of (a) Bi_2S_3 NRs (b) acid-modified M-CNTs, (c) TEM of CMHC-0.8. TEM images, (Inset: HR-TEM images of Bi_2S_3 NRs, M-CNTs and CMHC-0.8 respectively).

the defects present in the structure were analyzed. The morphology and microstructure of the as-prepared Bi_2S_3 NRs, M-CNTs, and CMHCs are compared in Fig. 3. The TEM image of Bi_2S_3 (NRs) shown in Fig. 3a. Inset Fig. 3a reveals a clear lattice fringe spacing of 0.33 nm, corresponding to the orthorhombic phase of Bi_2S_3. The M-CNTs were uniformly distributed due to the presence of high density functional groups such as carbonyl, hydroxyl, and carboxyls groups formed on the outer walls of the MWCNTs. The TEM image of the M-CNTs did not show functional groups, but it significantly highlights surface defects as evidence of functionalization (inset of Fig. 3b). Additionally, the as-synthesized CMHC displays a coaxial structure with a clear lattice fringe spacing of 0.39 nm (inset Fig. 3c). In case of CMHC, it can be clearly seen that the Bi_2S_3 NRs closely wrap over the M-CNT backbone (Fig. 3c).

To investigate the surface electronic states and chemical composition of the CMHC and Bi_2S_3 NRs, the XPS spectra was performed as shown in Fig. 4a and Fig. S2 respectively. Fig. 4a shows the XPS survey spectrum of CMHC and Bi_2S_3 NRs. Inset of Fig. 4 (a) shows the bare Bi_2S_3 NRs. All peaks can be assigned to C, O, Bi and S elements. The high-resolution XPS spectra of Bi_2S_3 NRs were shown in Figs. S2(a–b). Two strong peaks in the Bi region (Fig. S2a) at 158.5 eV and 163.6 eV, which corresponded to the Bi $4f_{7/2}$and Bi $4f_{5/2}$ peaks of the Bi^{3+} oxidation state, respectively. Another peak centered at 160.9 eV, corresponding to S2p for the S^{-2} oxidation states. The peak in the S region (Fig. S2b) at 225.6 eV could be assigned to S2s transition (Fig. S2 (b)). The presence of the C1s peak in the XPS spectrum of Bi_2S_3 can be attributed to the hydrocarbon deposition from the instrument. The ratio of peak integrations at the two regions Bi and S was measured to be 2:3, indicates the formation of Bi_2S_3. Moreover, the XPS survey spectrum of CMHC-0.8 contains all of the peaks of Bi_2S_3 and carbon peaks. Figs. S2c–d shows, C1s and O1s peaks centered at 284.6 eV and 526 eV, respectively. However, both of the peaks were significantly intensified in CMHC-0.8 due to the combination of Bi_2S_3 NRs and M-CNT (Fig. 4a.

XPS fitting of the deconvolution of C1s shown in Fig. S2 (c) was centered at 284.6 eV and other peaks representing acid-modified carbon atoms were also observed. The peak at 285 eV indicates the presence of sp^3 hybridized carbon atoms. Due to acid treatment, the DE convoluted C1s spectrum shows various oxygen groups. The peaks at 286, 287, and 290 eV are attributed to –C–O– (alcohol, ether), –C=O (ketone, aldehyde), and –COO– (carboxylic acid, ester), respectively. Likewise, the O1s spectrum (Fig. S2 (d)) could be integrated into two divergent peaks with binding energies of 531.8 and 533.9 eV originating from oxygen atoms bound to carbon atoms in the functional groups of alcohol (C-OH) and carboxylic acid (COOH), respectively [35,36]. Therefore, the abundant oxygen containing groups in the carbon composite will contribute to the improved catalytic activity towards the $I^{-}{}_{3}$ reduction.

Moreover, the phase components of the as-synthesized Bi_2S_3 NRs and with an optimized loading content were determined by XRD. The XRD pattern of the obtained Bi_2S_3 NRs shown in Fig. 4b. All the diffraction peaks can be readily indexed to the orthorhombic phase of Bi_2S_3 with lattice parameters of a = 11.17 Å, b = 11.31 Å, and c = 3.99 Å, corresponding to the standard pattern of Bi_2S_3 reported in the literature (JCPDS no.17-0320) [31]. No obvious characteristic peaks of other impurities were identified in the sample, demonstrating the purity of the Bi_2S_3 NRs produced by the solution process method. The XRD pattern of the CMHC-0.8 composite exhibits two additional peaks centered at 25.8° and 43° indexed to the (002) and (101) diffraction intensities, indicating a graphitic tubular structure [37]. The intensities of both peaks clearly indicate

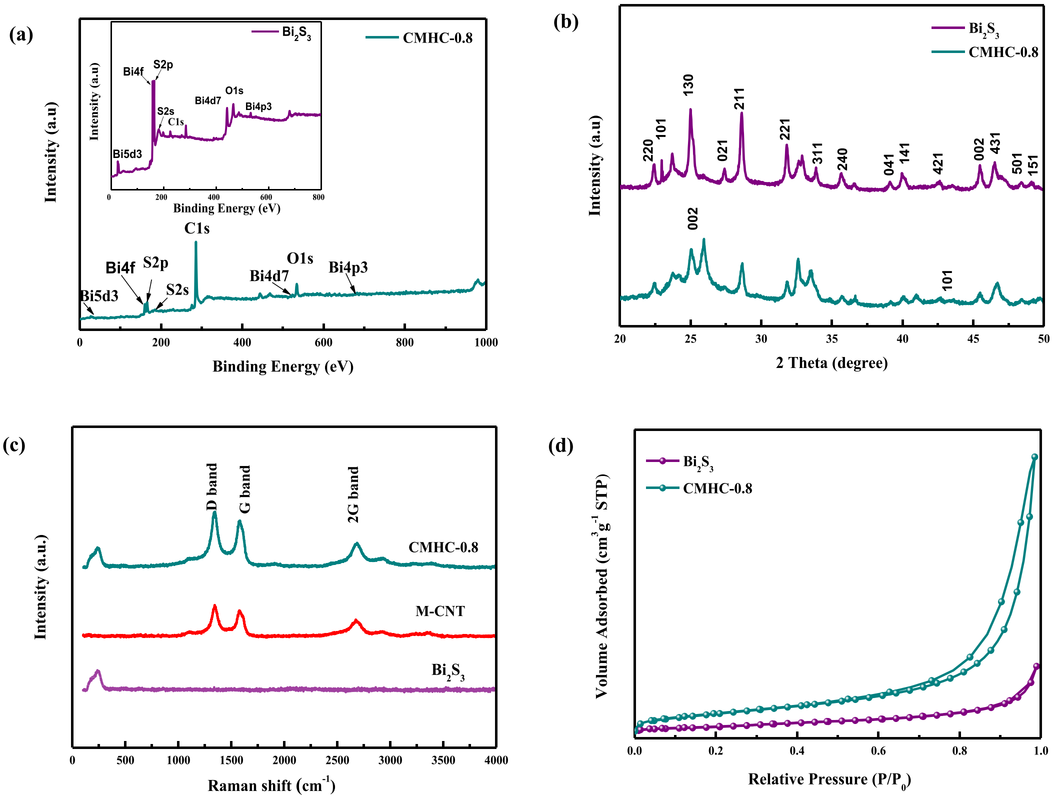

Fig. 4. (a) XPS Survey spectrum of CMHC 0.8 (inset XPS survey spectrum of Bi_2S_3 NRs), (b) XRD patterns of the as-prepared Bi_2S_3 and optimized CMHC-0.8 CE, (c) Raman spectra of Bi_2S_3 NRs, M-CNT, and CMHC obtained employing Bi_2S_3 NRs and M-CNT with a weight ratio of 0.8:1 in the wavelength range of 0–4000 cm^{-1} and (d) N_2 sorption-isotherms of the bare Bi_2S_3 NRs and CMHC-0.8.

that there was no loss of periodicity either in the inlayer or interlayer dimensions after acid modification of the MWCNTs. Therefore, based on the XRD spectrum, it is noteworthy that the characteristic features of the MWCNTs and Bi_2S_3 are well preserved in the CMHC.

The Raman spectra of the as-synthesized samples are presented in Fig. 4c. The solution-processed Bi_2S_3 NRs exhibited a crystalline structure, showing peaks at 143 cm^{-1}, 183 cm^{-1}, 235 cm^{-1}, and 252 cm^{-1}, which is consistent with previously reported data [38]. The CMHC-0.8 comprised of both acid-modified MWCNTs and solution-processed Bi_2S_3 NRs exhibited three additional peaks at 1347 cm^{-1} (D band), 1580 cm^{-1} (G band), and 2680 cm^{-1} (2D band) [39]. The D band corresponds to the disorder-induced phonon mode of sp^3 carbons, whereas the G band corresponds to the Raman-allowed phonon mode of sp^2 carbon. The features of the broad bands in the spectrum and the Raman intensity ratio of ~1.07 suggest a defect-rich structure of CMHC-0.8. The defect-rich structure of the composite is due to acid modification of the MWCNTs as well as the mesoporous structure of Bi_2S_3 NRs, which was further confirmed by Brunauer-Emmet-Teller BET analysis.

Furthermore, the Brunauer-Emmet-Teller (BET) specific surface area was determined by nitrogen adsorption-desorption measurements to provide further insight into the physical structure of the Bi_2S_3 NRs and CMHCs. Fig. 4 (d) shows the N_2 adsorption isotherms of the Bi_2S_3 NRs and CMHC-0.8. The textural properties of the as-synthesized materials are summarized in Table S2. As shown in Fig. 4d, both materials exhibit type IV isotherms with hysteresis according to the IUPAC classification, indicating the existence of abundant mesoporous structures in the material. Based on the hysteresis loop in the adsorption-desorption isotherm, the BET specific surface areas of the Bi_2S_3 NRs and CMHC-0.8 were 10.11 m^2/g and 22.93 m^2/g, respectively. The increment of the surface area is mainly due to the incorporation of acid-treated MWCNTs. Based on the N_2 desorption curve and Barrett-Joyner-Halenda BJH method, the average pore diameter of CMHC-0.8 was found to be 17.74 nm, corresponding to a mesoporous type [40]. The high specific surface area and pore diameter of CMHC-0.8 will effectively increase the accessibility of triiodide ions present in the electrolyte and speed up the reduction reaction of the quasi-solid electrolyte.

The electro catalytic activity and stability of the Bi_2S_3 NRs CE, M-CNT and CMHC-0.4, CMHC-0.8, CMHC-1.2 CE for iodide reduction in relation with a Pt CE are investigated using cyclic voltammetry (CV) and other electrochemical measurements with a symmetrical sandwich-type configuration. The CV spectra (Fig. 5a) for the various CE were performed at a scan rate of 20 mV s^{-1}. CV is a well-known electrochemical tool for analyzing the reaction kinetics and electro-catalytic activities of CE materials. A typical CV shows two sets of reduction-oxidation peaks at negative (Eq. (1)) and positive potentials (Eq. (2)), corresponding to the I_3^-/I^- and I_2/I_3^- couples, respectively [41].

$$I_3^- + 2e^- \rightarrow 3I^- \tag{1}$$

$$3I_2 + 2e^- \rightarrow 2I_3^- \tag{2}$$

The peak to peak voltage separation (E_{pp}) of the oxidation-reduction at lower potentials corresponds to the electro-catalytic activity of the CEs for $I^-/I^-{}_3$ redox reactions, where the standard electrochemical rate constant is conversely correlated. Furthermore, the cathodic peak current density (I_{CP}) and cathodic peak potential (E_{CP}) are also important parameters that illustrate a larger electroactive area and accelerated charge transfer at the electrode/electrolyte interface, both representative of the superior electro-catalytic activity of the CE material. For the CMHC-0.8 electrode, the cathodic peak current I_{CP} appears at −3.34 mA (Fig. 5a), which is much higher than the I_{CP} value of Pt (−0.68 mA). The higher peak current density value reveals that the CMHC-0.8 electrode features a high catalytic activity in the reduction of $I^-{}_3$ ions in the electrolyte, which is a paramount prerequisite for a robust CE to be applied in DSSCs. Additionally, the higher anodic peak current I_{AP} value of 3.5 mA indicates the superior electro conductivity of the as-synthesized CMHC-0.8 compared to the Pt electrode, which has an I_{AP} value of 0.88 mA. The peak to peak difference of CMHC-0.8 is 0.58 V and is comparable to Pt, which has a value of 0.33 V $E_{PP.}$ Thus, it is inferred that the designed CMHC is able to provide sufficient electro-catalytic sites for the operation of DSSCs. The electrochemical performances of CMHC-0.8 and Pt are illustrated in Table 1.

Fig. S3 (a) shows the successive CV curves for the CMHC-0.8 electrode measured at different scan rates ranging from 10 mV s^{-1} to 100 mV s^{-1} to analyze the effect of the scan rate with respect to the CV of CE. As the scan rate increased, the current densities were enhanced and furthermore, a shift of the potential peaks was also observed, proving the general electrochemical behavior of electrocatalytically active materials. The linear relationship between the anodic and cathodic peak currents and square root of the scan rate (Fig. S3 (b)) indicates the diffusion limitation of the redox reaction on the CMHC-0.8 electrode as well as homogenous coating of the composite on the substrate.

Furthermore, to evaluate the long term stability of CMHC-0.8 and Pt CEs towards the iodide/triiodide reduction reaction, we performed sequential CV for 30 cycles. As shown in the supplementary information (Fig. S3(c)), our proposed CMHC remained stable even after 30 cycles. This indicates the excellent electrochemical stability of our proposed composite CE whereas Pt showed a noticeable depletion of the peak current.

Fig. 5b shows electrochemical impedance spectroscopy (EIS) of the DSSCs using CEs with the films of Bi_2S_3 NRs, M-CNT, and CMHC-0.4, CMHC-0.8 and CMHC-1.2 CE and sputtered Pt. Symmetrical dummy cells based on two identical CEs of Bi_2S_3 NRs, M-CNT, and CMHC with different weight ratios and Pt were assembled for the EIS analyses. A schematic illustration of the symmetrical cells fabricated with CMHC is presented in Fig. S4. Typical Nyquist plots of the symmetrical cells are shown in Fig. 5b and the electrochemical parameters are summarized in Table 2. All of the EIS spectra were simulated using the EC-lab software and the equivalent circuit, as shown in Fig. S5 (a, b).

The equivalent circuit shown in Fig. S5(a) is used to interpret the impedance spectra of porous carbon materials. The equivalent circuit of carbon materials; slightly different from the conventional equivalent circuit of Pt, comprises of Constant phase Element (CPE) as a replacement of double layer capacitance due to the porous structure of the carbon electrodes and ($Z_{W\ Pore}$) Nernst diffusion impedance with in electrode pores, as altered by Roy Mayhew et al. [42]. The Nyquist plots of CMHC based symmetrical cells embody two semicircles: in high frequency range and low frequency range, respectively. The onset of first semicircle determines the ohmic serial resistance (R_S). The semicircle in the high frequency range represents the Nernst diffusion impedance resulting from diffusion within the electrode pores ($Z_{W\ Pore}$) and the second semicircle demonstrates the charge transfer resistance and the capacitance of the CMHC/electrolyte interface (R_{CT}, CPE).

Whereas, the conventional equivalent circuit designed by Hauch and Georg used for plane Pt is shown in Fig. S5 (b). The Nyquist plot of plane Pt typically exhibits two semicircles; one in the high frequency range representing the charge transfer resistance (R_{CT}) and one in low frequency range indicating the Nernst diffusion impedance (Z_d) [43]. Likewise, the onset of first semicircle in high frequency scan range indicates the ohmic serial resistance (R_S). In this research, we mainly focused on the series resistance (R_S) and charge transfer resistance (R_{CT}) to better understand the electrocatalytic performance of the CMHC CE.

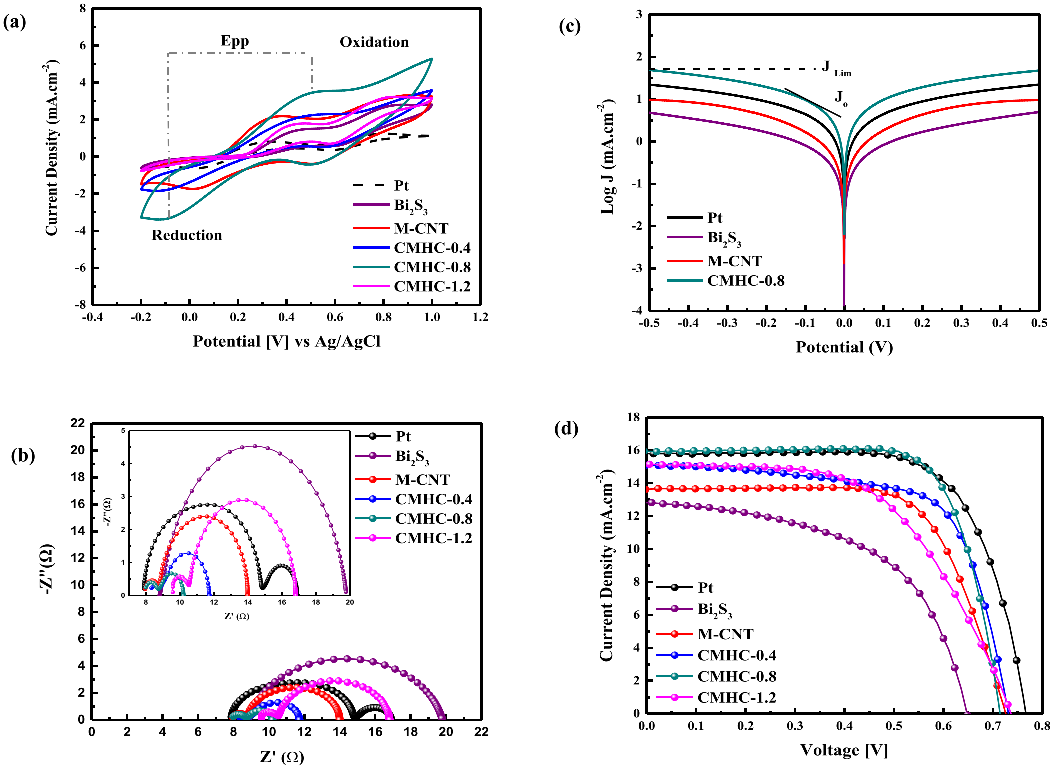

Fig. 5. (a) Cyclic voltammograms of as-prepared Pt, Bi_2S_3 NRs, M-CNT, and CMHC counter electrode obtained from with various Bi_2S_3 NRs weight ratios respectively (b)Nyquist plots of symmetrical dummy cells coated with Bi_2S_3 and different as-synthesized carbon composites (inset Nyquist plot of Pt based symmetrical dummy cell) (c) Tafel curve for Bi_2S_3, M-CNT, Pt and CMHC-0.8 counter electrodes and (d) Photovoltaic performances of QDSSCs based on Pt, Bi_2S_3 NRs, M-CNT, and different weight ratios of CMHC obtained at 100 mWcm^{-2}.

Table 1
Electrochemical performances of CMHC-0.8 and Pt-based CEs.

Counter Electrodes	I_{CP} [mA]	I_{AP} [mA]	E_{CP} [V]	E_{AP} [V]	E_{PP} [V]
CMHC-0.8	−3.34	3.5	−0.10	0.48	0.58
Pt	−0.68	0.88	0.04	0.33	0.33

The differences of the adhesion capability of the electro catalysts and FTO glass, and the conductivity of the different CEs are regarded as the reasons for the variations in sheet resistance of the electro catalysts. Bare Bi_2S_3 NRs exhibited the highest R_S (9.6 Ω) amongst all of the CEs, which was due to its poor adhesion on the FTO substrate. The low ohmic series resistance of the acid-modified MWCNTs reveals good bonding strength with the FTO glass.

Table 2
Electrochemical and photovoltaic performances of DSSCs fabricated with various CEs.

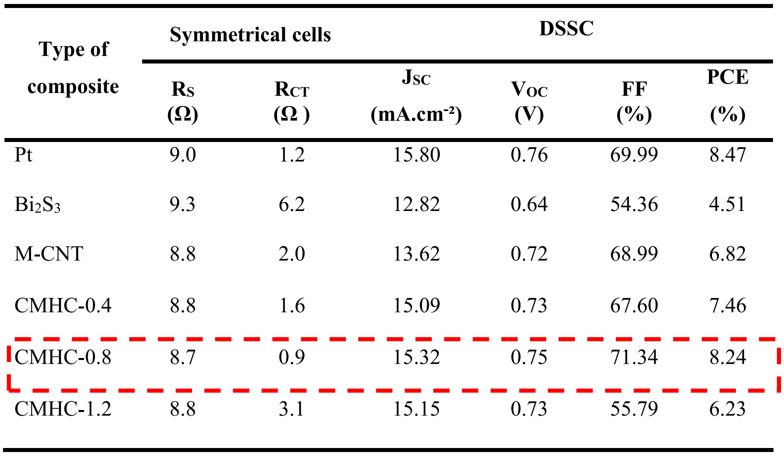

Type of composite	Symmetrical cells		DSSC			
	R_S (Ω)	R_{CT} (Ω)	J_{SC} (mA.cm^{-2})	V_{OC} (V)	FF (%)	PCE (%)
Pt	9.0	1.2	15.80	0.76	69.99	8.47
Bi_2S_3	9.3	6.2	12.82	0.64	54.36	4.51
M-CNT	8.8	2.0	13.62	0.72	68.99	6.82
CMHC-0.4	8.8	1.6	15.09	0.73	67.60	7.46
CMHC-0.8	8.7	0.9	15.32	0.75	71.34	8.24
CMHC-1.2	8.8	3.1	15.15	0.73	55.79	6.23

However, the charge transfer resistance was high. Our proposed electro catalyst, CMHC-0.8, has a very low R_S of 8.7 Ω and an R_{CT} of 0.9 Ω, which is much less than the values of bare Bi_2S_3, acid-treated MWCNTs, and conventional Pt. Stronger adhesion of CMHC-0.8 onto FTO leads to a low R_S value. Moreover, the lower R_{CT} value of our CE electro-catalyst implies a lower over potential for moving electrons from the CE to the electrolyte. The lower R_{CT} value of CMHC-0.8 confirms its high electro-catalytic activity. The lower charge transfer resistance is ultimately due to the synergistic effect of Bi_2S_3 NRs and acid-modified MWCNTs, resulting in a highly conductive, electro-catalytic active and defect-rich structure. It is interesting to note that the R_{CT} of different CMHCs decreased with increasing content of Bi_2S_3 from 0.4 g to 0.8 g, and then increased with further increases of the Bi_2S_3 content. Interestingly, the R_{CT} value of CMHC-0.8 was even lower than the Pt CE at 1.2Ω. This may be due the low surface area and porosity of Pt CE, which is not favorable for the reduction and proper absorption of gel electrolyte.

Tafel polarization characterization are usually used to study the electro-catalytic activity of the CEs for DSSCs.In order to confirm the electro catalytic activity of CEs with Pt and with various CEs, their Tafel polarization curves measurement were obtained using symmetrical cell at a scan rate of 20 mV s^{-1}. The Tafel polarization curves are shown in Fig. 5c. The Tafel curves of symmetrical cells based on CMHC-0.8 and Pt CEs show the logarithmic current density (log J) as a function of voltage (V). The Tafel curve is divided into three zones: the polarization zone at lower potentials, the Tafel zone in the middle, and the diffusion zone at higher voltages [44]. Amongst these zones, the Tafel zone corresponds to the electro-catalytic activity of the counter electrode. A larger slope was observed in the anodic and cathodic branches of the Tafel curve for CMHC-0.8 suggesting a higher current density (J_o) generated compared to Bi_2S_3 NRs, CMHC-0.4, CMHC-1.2 and Pt CEs This means that the CMHC-0.8 electrode has superior catalytic activity for $I^-{}_3$ reduction. J_o can be calculated using equation (3):

$$J_0 = \frac{RT}{nFR_{CT}} \tag{3}$$

where R_{CT} is the charge transfer resistance obtained from the EIS spectra, R is the gas constant, F is Faraday's constant, and n is the number of electrons exchanged in the reaction at the electrolyte and counter electrode interface [45]. R_{CT} and J_o have an inverse relationship, as is evident from equation (1). Combined with the EIS results, the CMHC-0.8 electrode shows a lower R_{CT} value, which is in good agreement with the Tafel polarization a measurement.

Considering the results obtained from CV, EIS, and Tafel polarization, the CMHC-0.8 catalyst displayed high catalytic activity towards reducing $I^-{}_3$, comparable to that of the Pt electrode. The promising results obtained by the EIS, CV, and Tafel polarization analyses suggest the excellent electro-catalytic activity of CMHC-0.8 in the $I^-/I^-{}_3$ mediator and its long-term electrochemical stability makes it a potential candidate to be used as a CE for DSSCs. To utilize this property, the as-synthesized CMHCs, bare Bi_2S_3 NRs, M-CNT, and conventional Pt were introduced as counter electrodes in the assembly of gel electrolyte-mediated DSSCs. The J-V curves of the corresponding cell devices measured under AM 1.5 illumination (1 sun, 100 mWcm^{-2}) are depicted in Fig. 5d and the related photovoltaic characteristics including the photocurrent density (J_{SC}), open circuit voltage (V_{OC}), fill factor (FF), and power conversion efficiency (η) are summarized in Table 2. The DSSC with the bare Bi_2S_3 CE yielded a low photo conversion efficiency of 4.55% due to its poor electrical conductivity, as observed in the CV results. As previously discussed in the EIS results, Bi_2S_3 has poor adhesion on the FTO substrate, which results in a high sheet resistance and ultimately low fill factor. The lower JSC of the Bi2S3 NRs is due to the very high charge transfer resistance, which is in accordance with the EIS results discussed in the previous section. The M-CNT CE-based DSSCs exhibited optimal performance with a J_{SC} of 13.62 mA cm^{-2}, V_{OC} of 0.72 V, FF of 68.99%, and photo conversion efficiency of 6.82%. The J_{SC} value of M-CNT was higher than the Bi2S3-based DSSC due to the 64% lower charge transfer resistance (R_{CT}) than Bi_2S_3 and comparatively superior electrical conductivity.

The combination of M-CNT and Bi_2S_3 resulted in improved photovoltaic performance. The photo conversion efficiency increased and then decreased by gradually increasing the concentration of Bi_2S_3 NRs in the composite. After optimization, the DSSC fabricated with CMHC-0.8 CE demonstrated a V_{OC} of 0.75 V, J_{SC} of 15.32 mA cm^{-2}, and FF of 71.34%, resulting in a high efficiency of 8.24%, which is greater than CMHC-0.4 and CMHC-1.2 CE (as summarized in Table 2) and comparable with efficiency of conventional Pt (8.47%). The higher J_{SC} achieved in the case of CMHC-0.8 is due to the low charge transfer resistance, indicating ease of charge transport [46]. Upon further increasing the concentration of bismuth sulfide NRs in the composite, a decreasing trend was observed in the J_{SC}, V_{OC}, and FF results and hence, the PCE decreased. This phenomenon may be attributed to the conglomeration of Bi_2S_3 in the composite. The larger aggregates formed upon increasing the concentration of bismuth sulfide prevent the charge transfer resistance [47] where a subsequent reduction of the J_{SC} value was observed.

A summary of the results obtained in this work and other reported literature involving Bi_2S_3-M-CNT (CMHC) based CE is compiled in Table S3. It is noteworthy to mention that CMHC CE synthesized by one pot has demonstrated remarkable performance in DSSCs and it is the first study of its so far.

9. Conclusion

In summary, we report the facile synthesis and application of a carbonous metallic heterostructure composite (CMHC) comprised of mild acid-treated MWCNTs and solution-processed Bi_2S_3 NRs as an efficient counter electrode material for quasi-solid state dye-sensitized solar cells. To the best of our knowledge, this is the first report of the application of an MWCNT and Bi_2S_3-based composite as a CE catalyst in QDSSCs. Initially, a highly conductive dispersion of MWCNTs with defects was formulated by mild acid treatment. Different concentrations of Bi_2S_3 NRs were combined with M-CNT to generate the CMHC and to produce a highly electro-catalytic active and electrical conductive electro-catalyst to be used as CEs in QDSSCs. The optimized CMHC-0.8 catalyst exhibited excellent electro-catalytic activity, stable redox activity, and outstanding electrochemical stability. The electrochemical analysis revealed a low R_{CT} value of 0.9 Ω for CMHC-0.8 in addition to its electro-catalytic activity with cyclic stability. Our proposed electro-catalyst achieved an overall efficiency of 8.24%, which is comparable to the Pt-based QDSSCs, which have an efficiency of 8.47%. The proposed facile synthesis technique of CMHC with a high efficiency and the sustainability of the QDSSCs demonstrate their promising utilization in dye-sensitized solar cells.

Acknowledgement

This work was funded by the Basic Science Research Program through the National Research Foundation of Korea (NRF) funded by the Ministry of Education (2012R1A6A1029029).

Appendix A. Supplementary data

Supplementary data related to this article can be found at https://doi.org/10.1016/j.electacta.2018.04.131.

References

[1] F. Lodermeyer, M. Prato, R. Costa, D. Guldi, Facile and quick preparation of carbon nanohorn-based counter electrodes for efficient dye-sensitized solar cells, Nanoscale 8 (2016) 7556–7561.

[2] H.-J. Hwang, S.-J. Joo, S.A. Patil, H.-S. Kim, Efficiency enhancement in dye-sensitized solar cells using the shape/size-dependent plasmonic nanocomposite photoanodes incorporating silver nanoplates, Nanoscale 9 (2017) 7960–7969.

[3] S. Casaluci, M. Gemmi, V. Pellegrini, A. Di Carlo, F. Bonaccorso, Graphene-based large area dye-sensitized solar cell modules, Nanoscale 8 (2016) 5368–5378.

[4] B. Kilic, S. Turkdogan, A. Astam, O.C. Ozer, M. Asgin, H. Cebeci, D. Urk, S.P. Mucur, Preparation of carbon nanotube/TiO2 mesoporous hybrid photoanode with iron pyrite (FeS2) thin films counter electrodes for dye-sensitized solar cell, Sci. Rep. 6 (2016).

[5] E. Bi, H. Chen, X. Yang, W. Peng, M. Grätzel, L. Han, A quasi core–shell nitrogen-doped graphene/cobalt sulfide conductive catalyst for highly efficient dye-sensitized solar cells, Energy Environ. Sci. 7 (2014) 2637–2641.

[6] S.-L. Chen, J. Tao, H.-J. Tao, Y.-Z. Shen, T. Wang, L. Pan, High-performance and low-cost dye-sensitized solar cells based on kesterite Cu2ZnSnS4 nanoplate arrays on a flexible carbon cloth cathode, J. Power Sources 330 (2016) 28–36.

[7] P. Dong, C.L. Pint, M. Hainey, F. Mirri, Y. Zhan, J. Zhang, M. Pasquali, R.H. Hauge, R. Verduzco, M. Jiang, H. Lin, J. Lou, Vertically aligned single-walled carbon nanotubes as low-cost and high electrocatalytic counter electrode for dye-sensitized solar cells, ACS Appl. Mater. Interfaces 3 (2011) 3157–3161.

[8] V.-Q. Nguyen, D. Schaming, P. Martin, J.-C. Lacroix, Highly resolved nanostructured PEDOT on large areas by nanosphere lithography and electrodeposition, ACS Appl. Mater. Interfaces 7 (2015) 21673–21681.

[9] A. Agresti, S. Pescetelli, E. Gatto, M. Venanzi, A. Di Carlo, Polyiodides formation in solvent based Dye Sensitized Solar Cells under reverse bias stress, J. Power Sources 287 (2015) 87–95.

[10] A. Hilmi, T.A. Shoker, T.H. Ghaddar, Universal low-temperature MWCNT-COOH-based counter electrode and a new thiolate/disulfide electrolyte system for dye-sensitized solar cells, ACS Appl. Mater. Interfaces 6 (2014) 8744–8753.

[11] A.A. Memon, A.A. Arbab, I.A. Sahito, N. Mengal, K.C. Sun, M.B. Qadir, Y.S. Choi, S.H. Jeong, Facile fabrication of activated charcoal decorated functionalized multi-walled carbon nanotube electro-catalyst for high performance quasi-solid state dye-sensitized solar cells, Electrochim. Acta 234 (2017) 53–62.

[12] A.A. Arbab, K.C. Sun, I.A. Sahito, M.B. Qadir, Y.S. Choi, S.H. Jeong, A novel activated-charcoal-doped multiwalled carbon nanotube hybrid for quasi-solid-state dye-sensitized solar cell outperforming Pt electrode, ACS Appl. Mater. Interfaces 8 (2016) 7471–7482.

[13] N. Mengal, I.A. Sahito, A.A. Arbab, K.C. Sun, M.B. Qadir, A.A. Memon, S.H. Jeong, Fabrication of a flexible and conductive lyocell fabric decorated with graphene nanosheets as a stable electrode material, Carbohydr. Polym. 152 (2016) 19–25.

[14] A.A. Memon, A.A. Arbab, I.A. Sahito, K.C. Sun, N. Mengal, S.H. Jeong, Synthesis of highly photo-catalytic and electro-catalytic active textile structured carbon electrode and its application in DSSCs, Sol. Energy 150 (2017) 521–531.

[15] S.A. Patil, N. Mengal, A.A. Memon, S.H. Jeong, H.-S. Kim, CuS thin film grown using the one pot, solution-process method for dye-sensitized solar cell applications, J. Alloys Compd. 708 (2017) 568–574.

[16] X. Cui, Z. Xie, Y. Wang, Novel CoS2 embedded carbon nanocages by direct sulfurizing metal-organic frameworks for dye-sensitized solar cells, Nanoscale 8 (2016) 11984–11992.

[17] X. Lin, M. Wu, Y. Wang, A. Hagfeldt, T. Ma, Novel counter electrode catalysts of niobium oxides supersede Pt for dye-sensitized solar cells, Chem. Commun. 47 (2011) 11489–11491.

[18] M. Wu, X. Lin, A. Hagfeldt, T. Ma, Low-cost molybdenum carbide and tungsten carbide counter electrodes for dye-sensitized solar cells, Angew. Chem. 123 (2011) 3582–3586.

[19] G.R. Li, J. Song, G.L. Pan, X.P. Gao, Highly Pt-like electrocatalytic activity of transition metal nitrides for dye-sensitized solar cells, Energy Environ. Sci. 4 (2011) 1680–1683.

[20] Q. Tai, B. Chen, F. Guo, S. Xu, H. Hu, B. Sebo, X.-Z. Zhao, In situ prepared transparent polyaniline electrode and its application in bifacial dye-sensitized solar cells, ACS Nano 5 (2011) 3795–3799.

[21] J. Burschka, V. Brault, S. Ahmad, L. Breau, M.K. Nazeeruddin, B. Marsan, S.M. Zakeeruddin, M. Grätzel, Influence of the counter electrode on the photovoltaic performance of dye-sensitized solar cells using a disulfide/thiolate redox electrolyte, Energy Environ. Sci. 5 (2012) 6089–6097.

[22] T. Liu, Y. Zhao, L. Gao, J. Ni, Engineering Bi 2 O 3-Bi 2 S 3 heterostructure for superior lithium storage, Sci. Rep. 5 (2015) 9307.

[23] A. Sajedi-Moghaddam, E. Saievar-Iranizad, M. Pumera, Two-dimensional transition metal dichalcogenide/conducting polymer composites: synthesis and applications, Nanoscale 9 (2017) 8052–8065.

[24] G.-r. Li, F. Wang, Q.-w. Jiang, X.-p. Gao, P.-w. Shen, Carbon nanotubes with titanium nitride as a low-cost counter-electrode material for dye-sensitized solar cells, Angew. Chem. Int. Ed. 49 (2010) 3653–3656.

[25] Y. Luo, Z. Gong, M. He, X. Wang, Z. Tang, H. Chen, Fabrication of high-quality carbon nanotube fibers for optoelectronic applications, Sol. Energy Mater. Sol. Cell. 97 (2012) 78–82.

[26] H. Lu, Q. Guo, F. Zan, H. Xia, Bi_2S_3 nanoparticles anchored on graphene nanosheets with superior electrochemical performance for supercapacitors, Mater. Res. Bull. 96 (2017) 471–477.

[27] Z. Zhang, C. Zhou, L. Huang, X. Wang, Y. Qu, Y. Lai, J. Li, Synthesis of bismuth sulfide/reduced graphene oxide composites and their electrochemical properties for lithium ion batteries, Electrochim. Acta 114 (2013) 88–94.

[28] Y. Zhao, T. Liu, H. Xia, L. Zhang, J. Jiang, M. Shen, J. Ni, L. Gao, Branch-structured Bi 2 S 3–CNT hybrids with improved lithium storage capability, J. Mater. Chem. 2 (2014) 13854–13858.

[29] P. Hu, Y. Cao, B. Lu, Flowerlike assemblies of Bi2S3 nanorods by solvothermal route and their electrochemical hydrogen storage performance, Mater. Lett. 106 (2013) 297–300.

[30] H. Zhang, L. Yang, Z. Liu, M. Ge, Z. Zhou, W. Chen, Q. Li, L. Liu, Facet-dependent activity of bismuth sulfide as low-cost counter-electrode materials for dye-sensitized solar cells, J. Mater. Chem. 22 (2012) 18572–18577.

[31] G. Li, X. Chen, G. Gao, Bi 2 S 3 microspheres grown on graphene sheets as low-cost counter-electrode materials for dye-sensitized solar cells, Nanoscale 6 (2014) 3283–3288.

[32] X.-Q. Zuo, X. Yang, L. Zhou, B. Yang, G. Li, H.-B. Tang, H.-J. Zhang, M.-Z. Wu, Y.-Q. Ma, S.-W. Jin, Facile synthesis of Bi 2 S 3–C composite microspheres as low-cost counter electrodes for dye-sensitized solar cells, RSC Adv. 4 (2014) 57412–57418.

[33] S.A. Patil, Y.-T. Hwang, V.V. Jadhav, K.H. Kim, H.-S. Kim, Solution processed growth and photoelectrochemistry of Bi 2 S 3 nanorods thin film, J. Photochem. Photobiol. A Chem. 332 (2017) 174–181.

[34] K.C. Sun, S.H. Yun, C.H. Yoon, H.H. Ko, S. Yi, S.H. Jeong, Enhanced power conversion efficiency of dye-sensitized solar cells using nanoparticle/nanotube double layered film, J. Nanosci. Nanotechnol. 13 (2013) 7938–7943.

[35] E.R. Edwards, E.F. Antunes, E.C. Botelho, M.R. Baldan, E.J. Corat, Evaluation of residual iron in carbon nanotubes purified by acid treatments, Appl. Surf. Sci. 258 (2011) 641–648.

[36] J. Kim, C.-l. Jung, M. Kim, S. Kim, Y. Kang, H.-s. Lee, J. Park, Y. Jun, D. Kim, Electrocatalytic activity of NiO on silicon nanowires with a carbon shell and its application in dye-sensitized solar cell counter electrodes, Nanoscale 8 (2016) 7761–7767.

[37] J. Balamurugan, A. Pandurangan, N.H. Kim, J.H. Lee, Facile synthesis of high quality multi-walled carbon nanotubes on novel 3D KIT-6: application in high performance dye-sensitized solar cells, Nanoscale 7 (2015) 679–689.

[38] M. Bernechea, Y. Cao, G. Konstantatos, Size and bandgap tunability in Bi2S3 colloidal nanocrystals and its effect in solution processed solar cells, J. Mater. Chem. 3 (2015) 20642–20648.

[39] W. Wei, K. Sun, Y.H. Hu, Direct conversion of CO 2 to 3D graphene and its excellent performance for dye-sensitized solar cells with 10% efficiency, J. Mater. Chem. 4 (2016) 12054–12057.

[40] S. Vadivel, A.N. Naveen, V.P. Kamalakannan, P. Cao, N. Balasubramanian, Facile large scale synthesis of Bi2S3 nano rods–graphene composite for photocatalytic photoelectrochemical and supercapacitor application, Appl. Surf. Sci. 351 (2015) 635–645.

[41] B. Anothumakkool, I. Agrawal, S.N. Bhange, R. Soni, O. Game, S.B. Ogale, S. Kurungot, Pt- and TCO-free flexible cathode for DSSC from highly conducting and flexible PEDOT paper prepared via in situ interfacial polymerization, ACS Appl. Mater. Interfaces 8 (2016) 553–562.

[42] J.D. Roy-Mayhew, D.J. Bozym, C. Punckt, I.A. Aksay, Functionalized graphene as a catalytic counter electrode in dye-sensitized solar cells, ACS Nano 4 (2010) 6203–6211.

[43] L.-H. Chang, C.-K. Hsieh, M.-C. Hsiao, J.-C. Chiang, P.-I. Liu, K.-K. Ho, C.-C.M. Ma, M.-Y. Yen, M.-C. Tsai, C.-H. Tsai, A graphene-multi-walled carbon nanotube hybrid supported on fluorinated tin oxide as a counter electrode of dye-sensitized solar cells, J. Power Sources 222 (2013) 518–525.

[44] I.A. Sahito, K.C. Sun, A.A. Arbab, M.B. Qadir, Y.S. Choi, S.H. Jeong, Flexible and conductive cotton fabric counter electrode coated with graphene nanosheets for high efficiency dye sensitized solar cell, J. Power Sources 319 (2016) 90–98.

[45] J. Wu, Z. Tang, Y. Huang, M. Huang, H. Yu, J. Lin, A dye-sensitized solar cell based on platinum nanotube counter electrode with efficiency of 9.05%, J. Power Sources 257 (2014) 84–89.

[46] M. Han, J. Jia, 3D Bi2S3/TiO2 cross-linked heterostructure: an efficient strategy to improve charge transport and separation for high photoelectrochemical performance, J. Power Sources 329 (2016) 23–30.

[47] In situ solution chemical reaction deposition of Bi2S3 quantum dots on mesoscopic TiO2 films for application in quantum dot sensitised solar cells, Mater. Technol. 31 (2016) 160–165.